RESEARCH ARTICLE

FASEB BioAdvances WILEY

Dopamine-related oxidative stress and mitochondrial dysfunction in dopaminergic neurons differentiated from deciduous teeth-derived stem cells of children with Down syndrome

Xiao Sun[1] | Hiroki Kato[2] | Hiroshi Sato[1] | Xu Han[1] | Yuta Hirofuji[1] |
Takahiro A. Kato[3] | Yasunari Sakai[4] | Shouichi Ohga[4] | Satoshi Fukumoto[1] |
Keiji Masuda[1]

[1]Section of Oral Medicine for Children, Division of Oral Health, Growth and Development, Faculty of Dental Science, Kyushu University, Fukuoka, Japan

[2]Department of Molecular Cell Biology and Oral Anatomy, Kyushu University Graduate School of Dental Science, Fukuoka, Japan

[3]Department of Neuropsychiatry, Graduate School of Medical Sciences, Kyushu University, Fukuoka, Japan

[4]Department of Pediatrics, Graduate School of Medical Sciences, Kyushu University, Fukuoka, Japan

Correspondence
Keiji Masuda and Satoshi Fukumoto, Section of Oral Medicine for Children, Division of Oral Health, Growth and Development, Faculty of Dental Science, Kyushu University, Maidashi 3-1-1, Higashi-Ku, Fukuoka 812-8582, Japan.
Emails: kemasuda@dent.kyushu-u.ac.jp; fukumoto@dent.kyushu-u.ac.jp

Abstract

Down syndrome (DS) is one of the common genetic disorders caused by the trisomy of human chromosome 21 (HSA21). Mitochondrial dysfunction and redox imbalance play important roles in DS pathology, and altered dopaminergic regulation has been demonstrated in the brain of individuals with DS. However, the pathological association of these elements is not yet fully understood. In this study, we analyzed dopaminergic neurons (DNs) differentiated from deciduous teeth-derived stem cells of children with DS or healthy control children. As previously observed in the analysis of a single case of DS, compared to controls, patient-derived DNs (DS-DNs) displayed shorter neurite outgrowth and fewer branches, as well as downregulated *vesicular monoamine transporter 2* and upregulated *dopamine transporter 1*, both of which are key regulators of dopamine homeostasis in DNs. In agreement with these expression profiles, DS-DNs accumulated dopamine intracellularly and had increased levels of cellular and mitochondrial reactive oxygen species (ROS). DS-DNs showed downregulation of non-canonical Notch ligand, *delta-like 1*, which may contribute to dopamine accumulation and increased ROS levels through *DAT1* upregulation. Furthermore, DS-DNs showed mitochondrial dysfunction in consistent with lower expression of peroxisome proliferator-activated receptor-gamma coactivator 1 alpha (PGC-1α) and upregulation of a HSA21-encoded negative regulator of

Abbreviations: APP, β-amyloid precursor protein; ATP, adenosine triphosphate; DAPI, 4′,6-diamidino-2-phenylindole; DAT1, dopamine transporter 1; DLK1, delta-like 1; DMR, differentially CpG methylated region; DN, dopaminergic neuron; DS, Down syndrome; DSCR1, Down syndrome candidate region-1; DYRK1A, dual-specificity tyrosine phosphorylation-regulated kinase 1A; FOXA2, forkhead box protein A2; HSA21, human chromosome 21; MAP2, microtubule-associated protein 2; MMP, mitochondrial membrane potential; NRIP1, nuclear receptor-interacting protein 1; NURR1, nuclear receptor-related 1; PGC-1α, peroxisome proliferator-activated receptor-gamma coactivator 1 alpha; PITX3, pituitary homeobox 3; PSD-95, postsynaptic density protein 95; ROS, reactive oxygen species; RT-qPCR, reverse transcription-polymerase chain reaction; SHED, stem cell from human exfoliated deciduous teeth; siRNA, small interference RNA; TH, tyrosine hydroxylase; VMAT2, vesicular monoamine transporter 2.

Xiao Sun and Hiroki Kato contributed equally to this work and are therefore co-first authors.

PGC-1α, *nuclear receptor-interacting protein 1*. These results suggest that dysregulated dopamine homeostasis may participate in oxidative stress and mitochondrial dysfunction of the dopaminergic system in DS.

KEYWORDS
dopaminergic neurons, Down syndrome, mitochondria, reactive oxygen species, stem cells from human exfoliated deciduous teeth

1 | INTRODUCTION

Mitochondrial dysfunction and oxidative stress have been commonly observed in several neurodevelopmental and neurodegenerative disorders, including down syndrome (DS).[1–4] DS is a common chromosomal aneuploidy disease and is caused by the trisomy of human chromosome 21 (HSA21), which affects multiple tissues, including the brain.[5,6] Although the underlying mechanisms of DS have not been fully determined, a dosage imbalance of HSA21-related genes and a resulting genome-wide dysregulation of gene expression due to epigenetic modifications have been proposed.[7–9] Many of these affected genes contribute to redox control and mitochondrial function.[1–4] Indeed, mitochondrial dysfunction and oxidative stress are involved in DS pathology, causing impaired neuronal development and maturation from early embryonic to adult stages.[6]

Dopaminergic neurons (DNs) in the midbrain originate from the mesodiencephalic floor plate and develop their neurites from fetal to adult stages, resulting in broadly distributed synaptic terminals in the brain regions involved in multiple functions, including reward, motor, and cognition.[10,11] Dysfunction of DNs has been found in autism spectrum disorder, attention deficit hyperactivity disorder and Alzheimer's disease, which are relatively frequent comorbidities in DS.[5,11–15] Previous studies of DS patient-derived postmortem brains and DS model mice have shown either increased or decreased dopamine concentrations, depending on the brain regions or age.[16–21] Thus, genetic and epigenetic factors associated with HSA21 trisomy may affect the development and function of the dopaminergic system. However, the exact pathology of the dopaminergic system remains elusive in DS, mainly because extensive analysis of the human brain has many limitations, particularly ethical concerns and restricted access to tissues.

Stem cells from human exfoliated deciduous teeth (SHEDs) are cranial neural crest-derived multipotent mesenchymal stem cells that express the neural stem cell marker, nestin, and have neurogenic potential.[22] Previous studies have shown that SHEDs can efficiently differentiate into DNs, making them a potential source of cell-based therapy for Parkinson's disease with DN degeneration.[23–25] DNs differentiated from patient-derived SHEDs have also contributed to elucidating dopamine-related pathologies in several neurodevelopmental disorders.[26–30] Previous analyses using SHEDs from a single case of DS pointed to impaired neurite development, downregulated *vesicular monoamine transporter2* (*VMAT2*) level, and upregulated *dopamine transporter1* (*DAT1*) level in DNs.[29] However, the pathological association between these defects remains unclear. In this study, to further elucidate the DN pathology of DS, the analysis was extended to three children with DS and three children with normal development, focusing on oxidative stress and mitochondria.

2 | MATERIALS AND METHODS

2.1 | SHED isolation, culture, and differentiation into DNs

Experiments using human samples were reviewed and approved by the Kyushu University Institutional Review Board for Human Genome/Gene Research (permission number: 678-03) and were conducted per the Declaration of Helsinki. Written informed consent was obtained from the parents of all participants. Deciduous teeth were collected from three typically developing boys (two 6-year-old boys and one 7-year-old boy) and three children with DS (6, 9, and 10-year-old boys).

SHED isolation and culture were performed as previously described.[26–29] Differentiation from SHEDs to DNs was based on a two-step procedure described by Fujii et al.[24] In the first step, 1.5×10^5 SHEDs were plated in a 6-well culture plate (Corning, NY, USA) and cultured in alpha modification of Eagle's Medium (Nacalai Tesque, Kyoto, Japan) with 15% fetal bovine serum (Sigma-Aldrich), 100 µM L-ascorbic acid 2-phosphate (Wako Pure Chemical Industries), 250 µg/ml fungizone (Thermo Fisher Scientific), 100 U/ml penicillin, and 100 µg/ml streptomycin (Nacalai Tesque). After 24 h, the cells were then cultured in Dulbecco's Modified Eagle's Medium (DMEM, Nacalai Tesque) supplemented with 20 ng/ml epidermal growth factor (Peprotech), 20 ng/ml

basic fibroblast growth factor (Peprotech), and 1% N2 supplement (Thermo Fisher Scientific) (first medium) for 2 days at 37°C in an incubator with 5% CO_2. In the second step, DMEM was replaced by neurobasal medium (Thermo Fisher Scientific) supplemented with 2% B27 supplement (Thermo Fisher Scientific), 1 mM dibutyryladenosine 3,5-cyclic monophosphate (Nacalai Tesque), 0.5 mM 3-isobutyl-1-methyl-xanthine (Wako Pure Chemical Industries), and 200 μM ascorbic acid (Nacalai Tesque) (second medium), and cells were incubated for 5 days at 37°C in an incubator with 5% CO_2. As previously reported, DNs were not fully matured at this stage to allow the strict discrimination between dendrites and axons.[29]

2.2 | Immunocytochemistry

DNs were cultured on the cover glass. They were fixed with 4% paraformaldehyde in 0.1 M sodium phosphate buffer (pH 7.4) for 10 min and were then permeabilized with 0.1% Triton X-100 in PBS for 5 min at room temperature. The cells were blocked with 2% BSA in PBS for 20 min and then incubated with the following primary antibodies for 90 min at room temperature: rabbit anti-Tom20 (#sc-11,415; Santa Cruz Biotechnology), mouse anti-β-tubulin III antibody (#T8578; Sigma-Aldrich), mouse anti-tyrosine hydroxylase (TH; #66334-1-Ig; Proteintech) and rabbit anti-dopamine (#ab6427; Abcam), followed by incubation with Alexa Fluor-conjugated secondary antibodies (Thermo Fisher Scientific) for 60 min at room temperature in the dark. Subsequently, nuclei were counterstained with 1 μg/ml of 4′,6-diamidino-2-phenylindole (DAPI) in PBS for 5 min at room temperature. The cover glass was then mounted on slides using ProLong Diamond mounting medium (Thermo Fisher Scientific). Fluorescence images were acquired using a Nikon C2 confocal microscope (Nikon).

2.3 | Analyses of neuronal morphology of DNs

Neuronal morphology and mitochondrial volume of DNs were assessed as previously described.[28] To measure the maximum neurite length and the total number of neurite branches, β-tubulin III-, and DAPI-stained pictures were acquired, and 30 cells of each control- and patient-derived case were analyzed with the Neurite Outgrowth module in MetaMorph software (Molecular Devices).

To analyze the purity of DNs in culture, five images stained with β-tubulin III and DAPI were taken from each control- and patient-derived culture. Cells with and without distinct neurites were counted. The number of cells with distinct neurites was divided by the total number of cells to determine the frequency of cells with neuron-like morphologies as the purity of DNs in culture.

2.4 | Western blotting

DNs were lysed with sample buffer (62.5 mM Tris–HCl buffer [pH 6.8] containing 2% sodium dodecyl sulfate [SDS], 5% β-mercaptoethanol, and 10% glycerol) and incubated at 95°C for 5 min. The proteins in the cell lysates were electrophoresed using SDS-polyacrylamide gel electrophoresis, and immunoblotting was performed using rabbit anti-nuclear receptor-related 1 (NURR1; #10975-2-AP; Proteintech), mouse anti-TH (#66334-1-Ig; Proteintech), rabbit anti-forkhead box protein A2 (FOXA2; #22474-1-AP; Proteintech), rabbit anti-peroxisome proliferator-activated receptor gamma coactivator 1 alpha (PGC-1α; #NBP1-04676; Novus Biologicals), mouse anti-postsynaptic density protein 95 (PSD-95; #MAB1598; Millipore), rabbit anti-paired-like homeodomain 3 (PITX3; #CSB-PA010844LA01HU; CUSABIO), mouse anti-microtubule-associated protein 2 (MAP2; #M9942; Sigma–Aldrich), rabbit anti-delta like non-canonical Notch ligand 1 (DLK1; #10636-1-AP; Proteintech), rabbit anti-DAT1; #22524-1-AP; Proteintech) and mouse anti-α-tubulin (#sc-32,293; Santa Cruz Biotechnology) antibodies. The immunoreactive bands were detected using ECL Prime (Cytiva) and analyzed using LAS-1000 pro (Fuji Film) and Image Gauge software (Fuji Film). α-tubulin was used as an internal control. To normalize the protein expression, the chemiluminescent signal was divided by the chemiluminescent signal of α-tubulin.

2.5 | Quantitative reverse transcription-polymerase chain reaction

Total RNA extraction and quantitative reverse transcription-polymerase chain reaction (RT-qPCR) were performed as previously described.[28] The sequence information of the primer sets used in this study is listed in Table 1. The relative expression of the target gene was analyzed using the comparative threshold cycle method by normalizing to *hypoxanthine phosphoribosyl transferase 1* expression.

2.6 | RNA interference

After the introduction of the cells back into the first medium, which was used for DNs differentiation, small

TABLE 1 Primers sequences

Gene	Sequence (5′-3′)
DAT1	
Forward	TGCTGCACAGACACCGTGAG
Reverse	AATGGTCCAGGAGCGTGAAGA
DLK1	
Forward	CGGGAAAGGACTGCCAGAAAAA
Reverse	GCAGAAATTGCCTGAGAAGCCA
HPRT1	
Forward	CCTGGCGTCGTGATTAGTG
Reverse	TCCCATCTCCTTCATCACATC
NRIP1	
Forward	TGACTGAAGGAGGACAGGGA
Reverse	TCTCCAAGCTCTGAGCCTCT
VMAT2	HA260638 (Takara Bio)

interference RNA (siRNA) transfection was then performed with Lipofectamine RNAiMAX (Thermo Fisher Scientific). The predesigned siRNAs were purchased from Sigma–Aldrich. The production numbers were SASI_Hs01_00049843 *for DLK*, SASI_Hs01_000609301 for *DAT1*, and SIC001-10NMOL for negative control.

To estimate knockdown efficiency, mRNA expression levels of target genes were measured by RT-qPCR. The knockdown efficiency of the target gene was calculated by setting the sample transfected with negative control siRNA into Ctrl-DN1 as 100%.

2.7 | Analysis of dopamine levels

To assess intracellular dopamine levels in DNs, images of dopamine and TH (as the cell area) staining were acquired, and 30 cells of each control- and patient-derived case were analyzed with the Multi Wavelengths Cell Scoring module in MetaMorph software. The dopamine signal intensity was divided by the TH-stained surface area.

Extracellular dopamine was measured using a Dopamine ELISA Kit (E-EL-0046, Elabscience) according to the manufacturer′s instructions. A culture medium (50 µl) was collected to measure extracellular dopamine. To measure extracellular dopamine under KCl stimulated conditions, the cells were treated with 50 mM KCl for 1 min at 37°C before harvesting the medium.

2.8 | Measurement of reactive oxygen species

To quantify cellular and mitochondrial reactive oxygen species (ROS) levels, cells were incubated with

5 µM CellROX Green (for cellular ROS; Thermo Fisher Scientific) or MitoSOX red (for mitochondrial ROS; Thermo Fisher Scientific) for 30 min. The cells were subsequently treated with TrypLE Express (Thermo Fisher Scientific) to detach them from the culture plate. The fluorescence signals of 10,000 cells were measured using a FACSCalibur instrument (BD Bioscience). The geometric means of the fluorescence signals were calculated using the Cell Quest software (BD Bioscience).

Mitochondrial ROS levels were determined using confocal microscopy as previously described.[31–33] In brief, cells were cultured in µ-dishes (Ibidi) and subsequently incubated with 5 µM MitoSOX Red (Thermo Fisher Scientific) and 20 nM MitoTracker Green FM (Thermo Fisher Scientific) for 30 min. Fluorescent images of MitoSOX Red and MitoTracker Green FM were acquired using a Nikon C2 confocal microscope. The fluorescence intensity of MitoSOX Red and MitoTracker Green FM was measured using the NIS-Elements software (Nikon). To determine mitochondrial ROS levels, the fluorescence intensities of MitoSOX Red were divided by that of MitoTracker Green FM.

2.9 | Measurement of mitochondrial membrane potential

Mitochondrial membrane potential (MMP) was measured using the MMP indicator JC-1 (Dojindo). DNs were incubated with 1 µM JC-1 for 10 min. Cells were then treated with TrypLE Express to detach them from the culture plates, and the cells were collected in tubes. JC-1 red and green signals were measured using a FACSCalibur. The geometric means of the red and green fluorescence intensities were calculated using Cell Quest software, and the ratio of red/green fluorescence was calculated.

2.10 | Analysis of intracellular adenosine triphosphate levels

Intracellular adenosine triphosphate (ATP) levels were measured as previously described.[28] Cells were harvested in ice-cold PBS, and the CellTiter-Glo Luminescent Cell Viability Assay (Promega) was subsequently used to measure intracellular ATP levels.

2.11 | Analyses of mitochondrial content and distribution in DNs

To evaluate mitochondrial contents in DNs, pictures of immunofluorescence staining for Tom20 (as the

mitochondrial area) and TH (as the cell area) were acquired and analyzed for 30 cells of each control- and patient-derived case using the Multi Wavelengths Cell Scoring module in MetaMorph software. The Tom20-stained area was divided by the TH-stained area to determine the total mitochondrial content in DNs for each case.

To evaluate mitochondrial distributions in neurites, the number of neurites in at least one Tom20-stained area and total neurites were manually counted for 30 randomly selected cells from the fluorescence images of each control- and patient-derived case. Thereafter, the number of neurites in at least one Tom20-stained area was divided by the total number of neurites to determine the proportion of mitochondria-containing neurites.

2.12 | Statistical analyses

Statistical analyses were performed using Student's *t*-tests with Prism9 (GraphPad). Values are presented as mean ± standard error of the mean (SEM). $p < 0.05$ was considered statistically significant. The results of RT-qPCR and western blotting experiments comparing patients and

typically developing boys were calculated with the results of a typically developing boy (Ctrl-SHED1 and Ctrl-DN1) set as 1.

3 | RESULTS

3.1 | Impaired neurite development and altered DN marker expression in patient-derived DNs (DS-DNs)

Fluorescent in situ hybridization analysis showed three copies of HSA21 in SHEDs obtained from three individuals with DS (Figure S1). More than 99% SHEDs in both groups expressed mesenchymal stem cell markers (CD44, CD73, and CD90) at comparable levels, and <1% SHEDs expressed CD34 and CD45 (hematopoietic markers) (Figure S2), as demonstrated by a previous study on SHED characterization.[34] SHEDs from the control and patient groups showed similar fibroblast-like morphologies, and the frequencies of colony-forming cells were comparable between the two groups (Figure S3). The SHEDs in both groups were differentiated into DNs (Figure 1A);
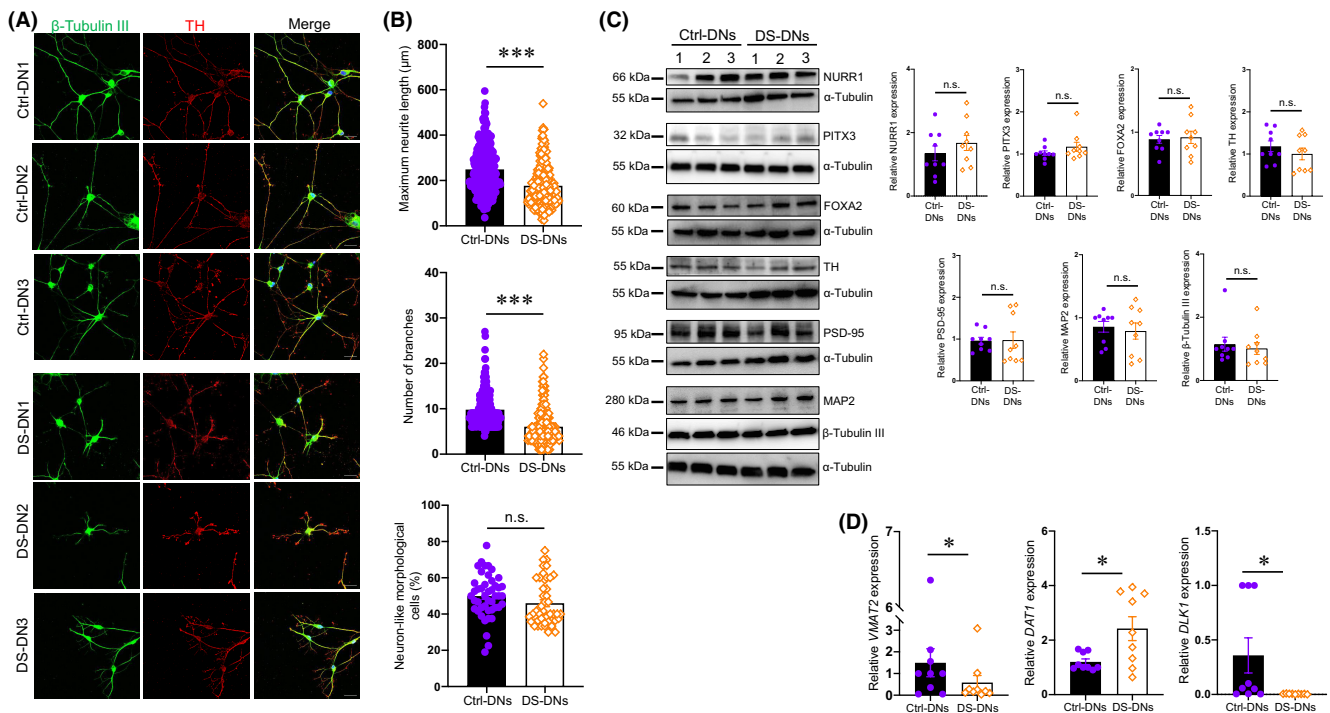

FIGURE 1 Impaired neurite development and altered mRNA expression in patient-derived dopaminergic neurons (DS-DNs). (A) DNs were stained with anti-β-tubulin III, anti-TH antibodies and 4′,6-diamidino-2-phenylindole dihydrochloride (DAPI) (nuclei). Scale bar = 25 μm. (B) Maximum neurite length and number of branches per cell and proportion of neuron-like cells are shown. The mean ± standard error of the mean (SEM) was calculated from three independent experiments. (C) Protein expression in DNs was analyzed by western blotting. The mean ± SEM was calculated from three independent experiments. (D) mRNA expression in DNs was measured using quantitative reverse transcription-polymerase chain reaction (RT-qPCR). The mean ± SEM was calculated from three independent experiments. *$p < 0.05$. ***$p < 0.001$

morphological analysis confirmed the previous data showing that both the maximum neurite length and the number of branches of DS-DNs were lower than those of control-derived DNs (Ctrl-DNs) (maximum neurite length: $t(538) = 8.796$, $p = 1.929 \times 10^{-17}$; the number of branches: $t(538) = 12.02$, $p = 1.16 \times 10^{-29}$; Figure 1B). The frequency of cells with neuron-like morphology was similar between the two groups ($t[88] = 1.532$, $p = 0.1292$; Figure 1B). Western blot analyses revealed comparable protein expression levels of NURR1, PITX3, FOXA2, and TH, critical markers for DN identity, as well as PSD-95, MAP2, and β-tubulin III, markers for mature neurons, between the two groups (NURR1: $t(16)=0.9871$, $p = 0.3383$; PITX3: $t(16)=1.245$, $p = 0.2311$; FOXA2: $t(16)=0.2775$, $p = 0.785$; TH: $t(16)=0.9637$, $p = 0.3495$; PSD-95: $t(16)=0.05905$, $p = 0.9536$; MAP2: $t(16)=0.4402$, $p = 0.6657$, β-tubulin III: $t(16) = 0.4682$, $p = 0.646$; Figure 1C). Considering that HSA21 trisomy may affect the expression of α-tubulin, β-actin was tested as another internal control for normalization (Figure S4). The lack of significant differences in

protein expression levels between the two groups indicated that both internal controls were valid for normalization in western blot analyses. As previously observed, VMAT2 was downregulated and DAT1 was upregulated (VMAT2: $t(16) = 2.204$, $p = 0.0425$; DAT1: $t(16) = 2.706$, $p = 0.01557$; Figure 1D).

Because DLK1 is a downstream target of NURR1 and is involved in the suppression of DAT1, we evaluated the relative expression of DLK1 in DS-DNs and Ctrl-DNs. DS-DNs showed lower DLK1 expression than Ctrl-DNs did ($t(16)=2.202$, $p = 0.0427$; Figure 1D). In addition, RNAi-mediated inhibition of DLK1 expression led to upregulation of DAT1 in Ctrl-DNs (DLK1 in Ctrl-DN1: $t(4) = 3.941$, $p = 0.0169$; DAT1 in Ctrl-DN1: $t(4) = 5.049$; DLK1 in Ctrl-DN2: $t(4) = 5.155$, $p = 0.0067$; DAT1 in Ctrl-DN2: $t(4) = 4.891$; DLK1 in Ctrl-DN3: $t(4) = 3.359$, $p = 0.0287$; DAT1 in Ctrl-DN3: $t(4) = 2.983$; Figure 2A,B), consistent with protein expression levels in the western blot analysis (DLK1: $t(16) = 2.188$, $p = 0.0439$; DAT1: $t(16)=2.527$, $p = 0.0224$; Figure 2C). These data suggest that the lower
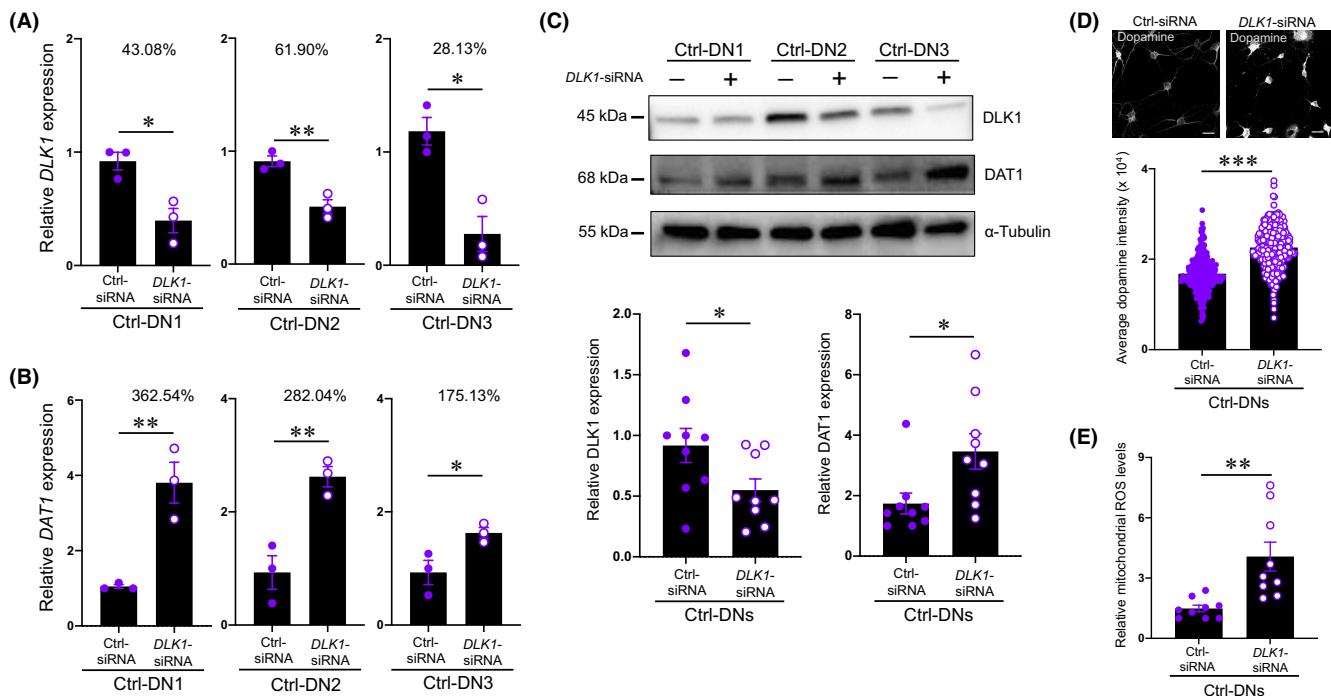

FIGURE 2 DAT1 upregulation in control-derived dopaminergic neurons (Ctrl-DNs) treated with small interference RNA (siRNA) for DLK1 silencing. Control stem cells from human exfoliated deciduous teeth (Ctrl-SHEDs) were transfected with negative control (Ctrl-siRNA) and DLK1 siRNA. (A, B) After differentiation into DNs, mRNA expression levels of DLK1 (A) and DAT1 (B) were measured using quantitative reverse transcription-polymerase chain reaction (RT-qPCR). Percent of DLK1 knock-down efficiency was represented in each graph (A). The mean ± standard error of the mean (SEM) was calculated from three independent experiments. (C) Protein expression levels in DNs were measured by western blotting. The mean ± standard error of the mean (SEM) was calculated from three independent experiments. (D) Intracellular dopamine levels in Ctrl-DNs treated with siRNA for DLK1 silencing. DS-DNs were stained with anti-dopamine antibodies. Images of DS-DN1 are shown as representative examples. Dopamine staining intensity per cell area was measured for 30 cells of each DS-DN. The mean ± SEM was calculated from three independent experiments. Scale bar = 25 μm. (E) Mitochondrial ROS levels in DNs were detected using MitoSOX Red. The signals were measured by flow cytometry. The mean ± standard error of the mean (SEM) was calculated from the three independent experiments. $*p < 0.05$, $**p < 0.01$, $***p < 0.001$

expression of *DLK1* is involved in the dysregulation of *DAT1* expression in DS-DNs.

To determine the mechanisms of *VMAT2* downregulation, we analyzed the CpG methylation status of its promoter region. We found no hypermethylated CpGs in the examined promoter region of *VMAT2* in DS-DNs ($t(4) = 0.950$, $p = 0.396$; Figure S5).

The numbers of surviving DNs were comparable between the two groups ($t(16) = 0.160$, $p = 0.8736$; Figure S6A); the finding is consistent with scarce detection of cleaved caspase-3-positive DNs in both groups, at least on day 8 ($t(16) = 0.296$, $p = 0.77548$; Figure S6B,C).

These results suggest that the extra HSA21 copy affects neurite development and dopamine regulation through modification of *DAT1* and *VMAT2* expression in DNs, rather than affecting the core differentiation pathway or cell survival. In addition, DLK1 may contribute to the negative regulation of DAT1 expression in DNs.

3.2 | Constitutive increase of intracellular dopamine levels associated with DAT1 upregulation in DS-DNs

To examine the effects of altered *DAT1* and *VMAT2* expression on dopamine homeostasis in DS-DNs, intracellular dopamine levels were analyzed by immunostaining with an anti-dopamine antibody. Baseline dopamine levels were higher in DS-DNs than in Ctrl-DNs ($t(538) = 9.543$, $p = 9.8 \times 10^{-5}$; Figure 3A). Stimulation with 50 mM KCl transiently reduced intracellular dopamine levels in both groups at comparable levels before recovery to baseline levels (0 min: $t(538) = 2.416$, $p = 0.016$; 1 min: $t(538) = 0.871$, $p = 0.3841$; 10 min: $t(538) = 1.329$, $p = 0.1848$; 30 min: $t(538) = 2.143$, $p = 0.0325$; Figure 3B,C). The rate of reduction in intracellular dopamine levels at 1 min after stimulation was 52.6% for DS-DNs and 43.9% for Ctrl-DNs (Figure 3C). These data were compatible
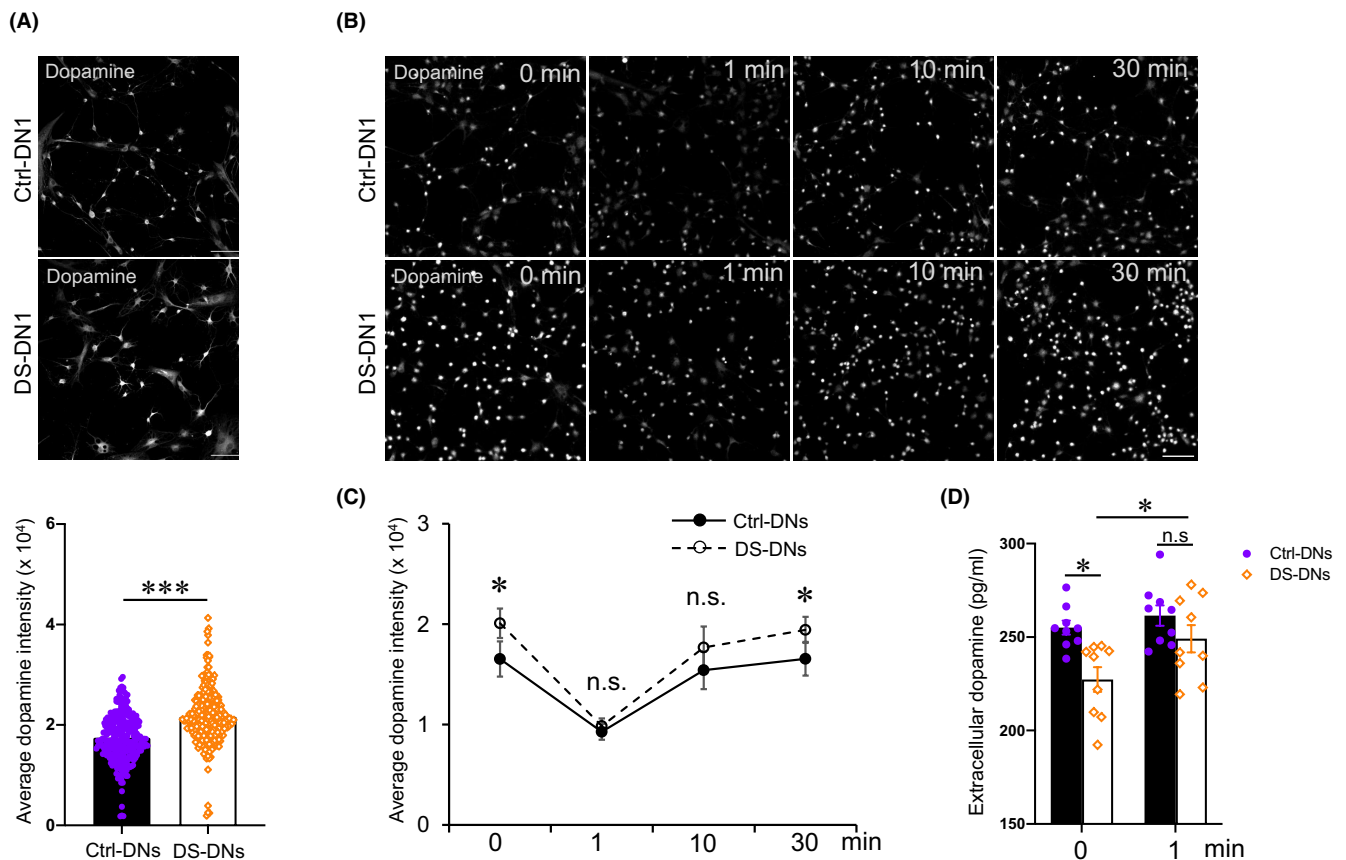

FIGURE 3 Altered dopamine levels in patient-derived dopaminergic neurons (DS-DNs). (A) DNs were stained with anti-dopamine antibodies. Scale bar = 25 μm. Dopamine staining intensity per cell area was measured for 30 cells of each control-derived dopaminergic neurons (Ctrl-DN) and DS-DN case. The mean ± standard error of the mean (SEM) was calculated from three independent experiments. (B) DNs were stimulated with 50 mM KCl for indicated times and then subsequently stained with anti-dopamine antibodies. Scale bar = 100 μm. The dopamine staining picture of Ctrl-DN1 (upper panel in A and B) and DS-DN1 (lower panel in A and B) are shown as representative examples. (C) Dopamine staining intensity per cell area in (B) was measured for 30 cells of each control-derived dopaminergic neuron (Ctrl-DN) and DS-DN case. The mean ± SEM was calculated from three independent experiments. (D) Extracellular dopamine levels of Ctrl-DNs and DS-DNs were measured under basal conditions and a 50 mM KCl stimulated condition. The mean ± standard error of the mean (SEM) was calculated from three independent experiments. *$p < 0.05$, ***$p < 0.001$

with extracellular dopamine levels at 0 and 1 min after stimulation (0 min: $t (16) = 3.644$, $p = 0.0022$; 1 min: $t (16) = 1.359$, $p = 0.193$; Figure 3D). In DS-DNs, extracellular dopamine levels were elevated in response to KCl ($t (16) = 2.209$, $p = 0.0421$; Figure 3D).

The possible role of upregulated *DAT1* in the basal accumulation of intracellular dopamine in DS-DNs was assessed by RNAi-mediated inhibition of *DAT1* expression (Figure 4). The treatment with siRNA for *DAT1* inhibited *DAT1* expression ($t (16) = 2.317$, $p = 0.0341$; Figure 4A). Protein expression of DAT1 was confirmed by western blotting (Figure 4B). This treatment reduced intracellular dopamine levels in DS-DNs, compared to Ctrl-siRNA treatment ($t(538) = 6.84$, $p = 2.16 \times 10^{-11}$; Figure 4C). Conversely, *DAT1* upregulation through *DLK1* inhibition resulted in intracellular dopamine accumulation in Ctrl-DNs ($t(538) = 15.57$, $p = 2.24 \times 10^{-45}$; Figure 2D).

These results suggest that DS-DNs have constitutively high intracellular dopamine levels at the basal condition associated with *DAT1* upregulation and no apparent defects in the stimulation-induced transient and acute release of dopamine.

3.3 | Dopamine-related ROS elevation and mitochondrial dysfunction in DS-DNs

Elevated ROS levels have been documented as playing an important role in the pathology of DS and cytosolic dopamine is an endogenous source of ROS. We examined the possibility that intracellular dopamine accumulation is involved in elevated ROS levels in DS-DNs. The total ROS sensor, CellROX Green, detected higher ROS signals in DS-DNs than in Ctrl-DNs ($t (16) = 4.786$, $p = 0.0002$; Figure 5A). The fluorescence intensity of
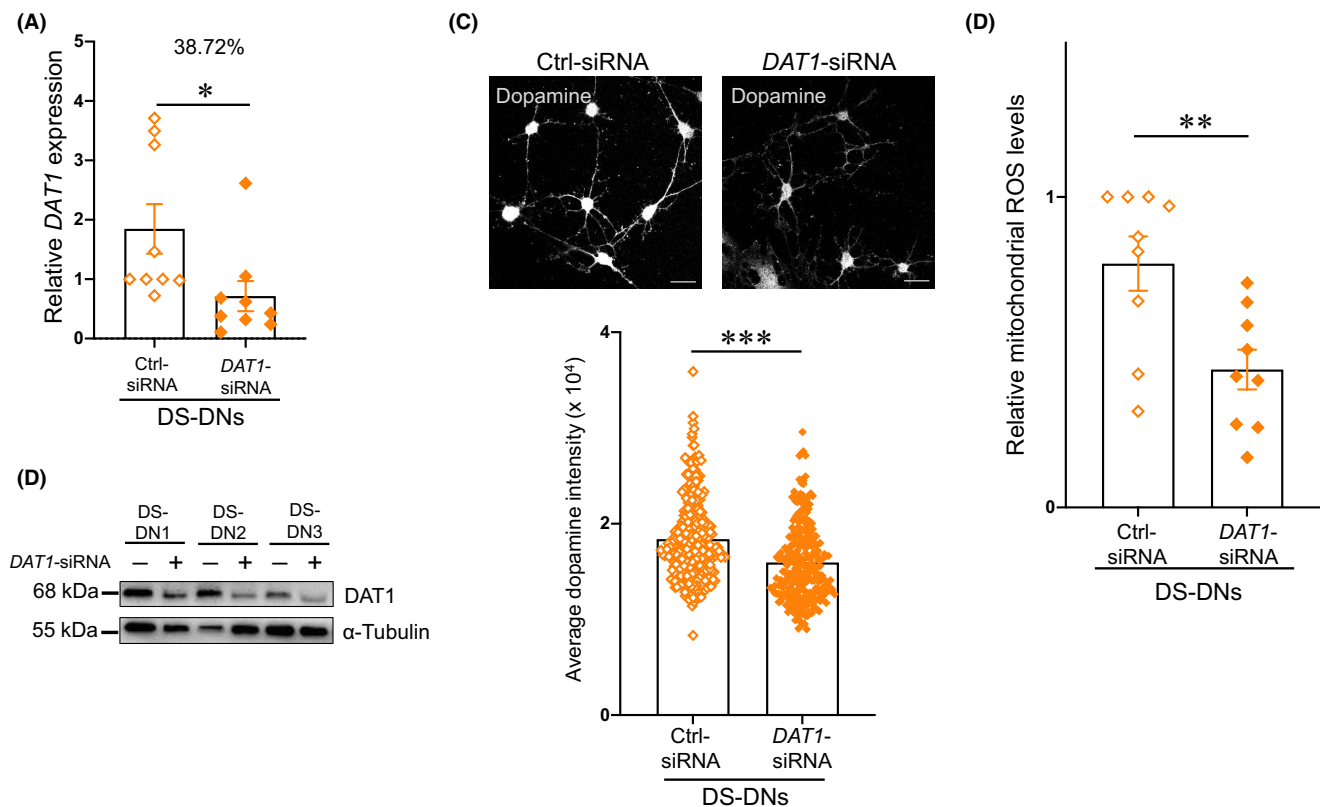

FIGURE 4 Downregulation of intracellular dopamine levels in patient-derived dopaminergic neurons (DS-DNs) treated with small interference RNA (siRNA) for *DAT1* silencing. Patient-derived stem cells from human exfoliated deciduous teeth (DS-SHEDs) were transfected with negative control (Ctrl-siRNA) and *DAT1* siRNA. (A) After differentiation into DNs, mRNA expression levels of *DAT1* were measured using quantitative reverse transcription-polymerase chain reaction (RT-qPCR). Percent of *DAT1* knock-down efficiency was shown in the graph. The mean ± standard error of the mean (SEM) was calculated from three independent experiments. (B) Protein expression of DAT1 was confirmed by western blotting. (C) Each DS-DNs was stained with anti-dopamine antibodies. Images of DS-DN1 are shown as representative examples. Dopamine staining intensity per cell area was measured for 30 cells of each DS-DNs. The mean ± standard error of the mean (SEM) was calculated from three independent experiments. Scale bar = 25 µm. (D) Mitochondrial ROS levels in each DS-DNs were detected using MitoSOX Red. The signals were measured using flow cytometry. The mean ± standard error of the mean (SEM) was calculated from the three independent experiments. *$p < 0.05$. **$p < 0.01$. ***$p < 0.001$
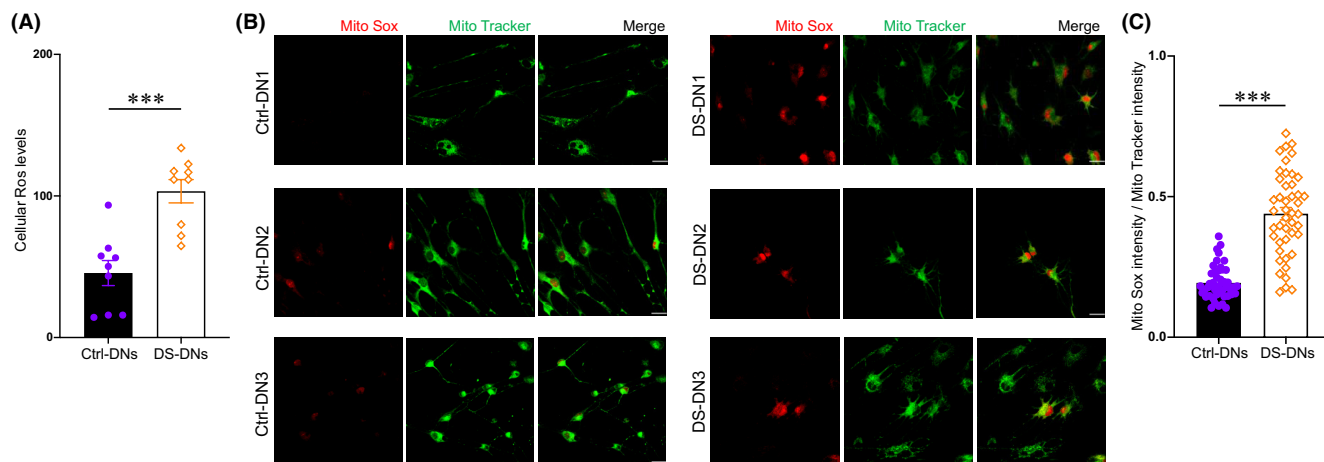
(A)

(B)

(C)

FIGURE 5 Increased reactive oxygen species (ROS) levels in patient-derived dopaminergic neurons (DS-DNs). (A) Cellular ROS levels were measured with Cell ROX green. DNs were stained with Cell ROX green, and the signal was measured using flow cytometry. The mean ± standard error of the mean (SEM) was calculated from the three independent experiments. ***p <0.001. (B) Mitochondrial ROS was detected using MitoSOX Red. DNs were stained with MitoSOX Red and MitoTracker Green FM. Scale bar = 25 μm. (C) Fluorescence intensity of MitoSOX Red and MitoTracker Green FM were measured from five images of each Ctrl-DN and DS-DN case, and the intensity of MitoSOX Red was divided by that of MitoTracker Green FM. The mean ± SEM was calculated from three independent experiments

MitoSox Red relative to that of MitoTracker Green for evaluating mitochondrial ROS levels was also higher in DS-DNs than in Ctrl-DNs ($t[88] = 4.338$, $p = 3.8 \times 10^{-5}$; Figure 5B,C). Mitochondrial ROS was reduced in DS-DNs with decreased intracellular dopamine by *DAT1* inhibition ($t(16) = 3.154$, $p = 0.0061$; Figure 4D). Conversely, Ctrl-DNs with upregulated *DAT1* by *DLK1* inhibition showed elevated ROS levels ($t(16) = 3.502$, $p = 0.0029$; Figure 2E). Both cellular and mitochondrial ROS levels were comparable in the two groups before differentiation (cellular ROS: $t(16)=1.559$, $p = 0.13845$; mitochondrial ROS: $t(88) = 1.023$, $p = 0.30888$; Figure S7A–C). Together, these findings indicate that intracellular dopamine accumulation may contribute to ROS elevation during the differentiation of DS-DNs.

Since impaired neurite development and higher ROS levels were observed in DS-DNs, we further analyzed mitochondrial function, which is critical for neurite development and is also sensitive to ROS damage. Both MMP and ATP levels, which indicate mitochondrial oxidative phosphorylation activity, were lower in DS-DNs than in Ctrl-DNs (MMP: $t(16)= 5.145$, $p = 1.079 \times 10^{-6}$; ATP: $t(16)=7.596$, $p = 9.77 \times 10^{-5}$; Figure 6A,B). The expression of *nuclear receptor-interacting protein 1* (*NRIP1*), a HSA21-encoded suppressor of mitochondrial biogenesis, was higher in DS-DNs than in Ctrl-DNs ($t(16)=2.869$, $p = 0.01112$; Figure 6C). Western blot analysis showed that the expression of PGC-1α, a master regulator of mitochondrial biogenesis, was reduced in DS-DNs compared to that in Ctrl-DNs ($t(16) = 2.812$, $p = 0.01252$; Figure 6D). Mitochondrial content per cell area and proportion of neurites containing mitochondria were lower in DS-DNs than in Ctrl-DNs (Tom20-stained area per cell area:

$t(538) = 15.12$, $p = 1.001 \times 10^{-6}$; proportion of neurites containing mitochondria: $t(538) = 14.45$, $p = 2.86 \times 10^{-7}$; Figure 6E–G, Figure S8). Collectively, these data suggest defects of mitochondrial ATP production, redox control, and biogenesis in DS-DNs.

4 | DISCUSSION

In this study, SHEDs were obtained from children with DS and were differentiated into DNs in vitro to elucidate the neuropathology of DS. DS-DNs showed no apparent defects in their differentiation; however, they exhibited impaired neurite development and altered expression of *DAT1* and *VMAT2*, as previously reported in the analysis of a single case of DS.[29] We also found that *DAT1* upregulation via *DLK1* downregulation may be implicated in dopamine accumulation and ROS elevation in DS-DNs. Dopamine dysregulation may participate in oxidative stress and mitochondrial dysfunction associated with developmental defects of the dopaminergic system in DS patients.

The cell biological basis underlying functional deficits in the dopaminergic system in patients with DS has not been fully elucidated, although extensive evidence indicates altered dopamine levels in these patients. Decreased levels of dopamine and its metabolites have been detected in the urine in individuals with DS,[35] in the frontal cortex in human fetuses with DS,[36] and the striatal regions in postmortem adult human DS brains.[16,20] Other studies have reported increased levels of dopamine and its metabolites in the cortex, limbic regions, and cerebellum in postmortem human DS brains[17,20]; in the cerebrospinal fluid
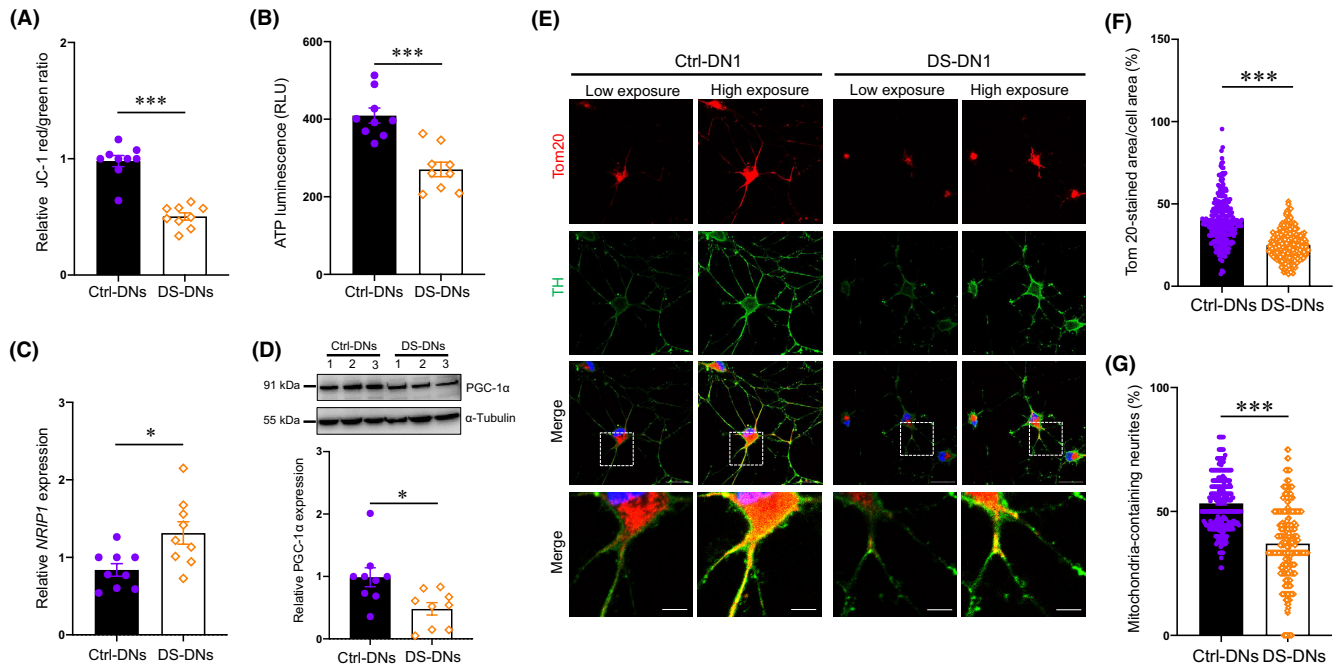
FIGURE 6 Impaired mitochondrial functions in patient-derived dopaminergic neurons (DS-DNs). (A) Mitochondrial membrane potential was measured with JC-1. JC-1 red and green signals were measured using flow cytometry. The ratio of JC-1 red/green was calculated. The mean ± standard error of the mean (SEM) was calculated from three independent experiments. (B) ATP levels were measured using luminescence assays. ATP luminescence signals were divided by the number of cells. The mean ± SEM was calculated from three independent experiments. (C) *NRIP1* mRNA expression in DNs was measured using quantitative reverse transcription-polymerase chain reaction. The mean ± SEM was calculated from three independent experiments. (D) PGC-1α protein expression levels were measured by western blot analysis. The mean ± SEM was calculated from three independent experiments. *$p < 0.05$, ***$p < 0.001$. (E) Representative images of mitochondrial content and distribution in DNs. DNs were stained with anti-Tom20 (a mitochondrial marker) and anti-TH antibodies and counterstained with 4′,6-diamidino-2-phenylindole dihydrochloride (DAPI). Scale bar = 25 μm. Details of the boxed region in the merged images are shown in the bottom panel. Scale bar = 100 μm. (F, G) Mitochondrial-stained area/cell area (upper panel) and the percentage of mitochondria-containing neurites (lower panel) were measured for 30 cells of each control-derived (Ctrl)- and patient-derived (DS) case. The mean ± standard error of the mean was calculated from three independent experiments. ***$p < 0.001$

in DS patients[36]; and in the striatum in a mouse model of DS.[21] Another study using mouse models suggested that aging may be an additional factor in bidirectional and brain region-specific alterations in dopamine levels.[19] In the current analysis, together with our previous data,[29] DS-DNs showed shorter neurites with fewer branches than Ctrl-DNs, but there were no apparent differences in cell death-associated signals between DS-DNs and Ctrl-DNs. This suggests that the brains of individuals with DS may contain fewer synaptic terminals of the dopaminergic system. DS-DNs also exhibited constitutively elevated baseline levels of intracellular dopamine, but their dopamine secretion was still transiently accelerated by stimulation. Conversely, the DS brain might be characterized by a higher content of dopamine in DNs. Therefore, the variability of dopamine levels previously reported in different samples might reflect the age and regional differences in the distribution of DNs in the brain in patients with DS.

Potential molecules associated with this variability may be upregulated *DAT1* and downregulated *VMAT2*

in DS-DNs, which can alter intracellular dopamine homeostasis. However, the expression of these two genes is directionally paralleled during DN development by tight regulation with several elements.[10] NURR1 and PITX3 are two core transcription factors that functionally interconnect in DN development.[37–39] These transcription factors positively regulate both *DAT1* and *VMAT2* expression required for DN specification.[37,38] DS-DNs and Ctrl-DNs displayed comparable expression levels of not only NURR1 and PITX3 but also TH, which is another target gene of NURR1 and PITX3,[37] suggesting no critical defect in the basic function of these transcription factors. Considering the contra-directional dysregulation of *DAT1* and *VMAT2* expression in DS-DNs, additional elements might be involved in differential regulation of *DAT1* and *VMAT2* expression during DN development.

In DS-DN, DLK1 was downregulated, which might contribute to the DAT1 upregulation. DLK1 is a transmembrane glycoprotein that is expressed in a variety of cell types and contributes to their differentiation

primarily via the Notch signaling pathway, although its molecular mechanisms have not been yet fully understood.[40–44] The extracellular domain of DLK1 has a DOS (Delta and OSM-11) domain but lacks a DSL (Delta/ Serrate/LAG-2) domain, both of which are specific components of canonical Notch ligands. Therefore, DLK1 is structurally classified into a non-canonical Notch ligand. The DLK1 extracellular domain cleaved by protease also functions as a soluble ligand. In vitro analyses show that exogenous soluble Dlk1 has a positive effect on the proliferation of DN progenitors, but in subsequent differentiation stages, expression of endogenous Dlk1 is required for the acquisition of dopaminergic phenotypes of DN precursors.[45] In vivo studies using Nurr1-deficient and Dlk1-deficient mice show that Dlk1 is the downstream target of Nurr1 and blocks premature Dat expression in DN precursors.[39] Therefore, NURR1 regulates the expression of both DAT1 and DLK1, and DLK1 may further modulate the expression of DAT1 during DN development. Other studies have demonstrated altered expression of genes encoding Notch signaling elements in DS.[46–49] Defects in the DLK1-mediated signal pathway may contribute to the DAT1 upregulation in DS-DNs, which may be involved in dopamine accumulation and increased ROS levels.

The exact mechanisms of DLK1 downregulation in DS-DNs remain unclear. In mice, Pitx3 activates Nurr1 by inhibiting the histone deacetylase in the Nurr1 transcription complex to induce many target genes such as *Th* and *Vmat2*, but Pitx3 specifically downregulates *Dlk1* expression.[39] These data suggest that additional regulatory elements may contribute to *DLK1* expression. This possibility is also supported by current data showing that *DLK1* was downregulated with no apparent defects in both NURR1 and PITX3 expression in DS-DNs. Potential elements involved in *DLK1* expression may be affected by the extra HSA21. The imprinted *DLK1* locus may represent another target affected by the extra HSA21. *DLK1* is located in the DLK1-DIO3 gene cluster on the human chromosome 14 and is activated from the paternally inherited chromosome.[50] Differentially CpG methylated regions (DMRs) involved in *DLK1* expression have been identified in this locus. Dysregulated methylation of the DMRs blocks *DLK1* expression, which is associated with severe growth defects such as Temple syndrome.[51] In DS, tissue- or cell type-specific epigenetic alterations in the whole genome, particularly differential DNA methylation, have been reported.[8,9,52,53] Altered methylation of these DMRs may contribute to *DLK1* downregulation in DS-DNs.

We speculated that an altered DNA methylation status might also contribute to *VMAT2* downregulation in DS-DNs. DNA hypermethylation of the *VMAT2* promoter has been demonstrated to be correlated with its downregulation in human prostate cancer.[54,55] However, no hypermethylated CpG pattern was observed in the examined promoter region of *VMAT2* in DS-DNs. Therefore, unidentified transcriptional cofactors or other epigenetic mechanisms associated with HSA21 trisomy might regulate *VMAT2* expression in DS-DNs.

Mitochondrial dysfunction and oxidative stress have been reported in DS.[2–4] We also observed accumulation of both intracellular and mitochondrial ROS in patient-derived cultured DNs. The current data suggest that altered *DAT1* and *VMAT2* expression is associated with excessive ROS generation through dopamine dysregulation in DS-DNs. DAT1 is critical for transporting extracellular dopamine to the cytosol of dopaminergic presynaptic terminals.[56] VMAT2 is critical for packing oxidation-sensitive cytosolic dopamine into vesicles to minimize dopamine oxidation.[57,58] Thus, the combination of upregulated *DAT1* and downregulated *VMAT2* might contribute to ROS overproduction through the accumulation of cytosolic free dopamine.[59,60] DS-DNs also showed decreased mitochondrial activity and biogenesis, which are possibly associated with HSA21 trisomy-related impairment of the NRIP1/PGC-1α axis in mitochondrial biogenesis, as previously reported in other cell types.[61–63] Although it is necessary to further analyze mitochondrial elements impaired by ROS, including respiratory chain complex activity and mitochondrial DNA damage in DS-DNs, dysregulation of dopamine compartmentalization may represent an additional element of oxidative stress and mitochondrial dysfunction, leading to developmental defects of the dopaminergic system in the DS brain.

Defects in neurite development of DS-DNs are shown, which may reflect the aspects of dendrite pathology, including marked reductions in dendritic complexity and in spine density which are commonly observed in DS. *Dual-specificity tyrosine phosphorylation-regulated kinase 1A* (*DYRK1A*), *Down syndrome candidate region-1* (*DSCR1*), and *β-amyloid precursor protein* (*APP*) on HSA21 have been extensively studied as dose-dependent genes associated with dendrite pathology in DS.[6,64] Mitochondria also contribute to the neuroplasticity through energy production, Ca^{2+} regulation and redox homeostasis, which are impaired in DS.[2–4,65] Non-human hippocampal and cortical pyramidal neurons have been shown to be useful models for these researches. Dendritic development in individual neurons is also regulated in a subtype-specific manner, which depends not only on the endogenous elements of the neuron but also on extracellular elements such as presynaptic activity.[66] In the dopaminergic system with dopamine as an effector, endogenous dopamine dysregulation, along with altered extracellular cues from other neuron subtypes, may affect the dendritic development of DNs. Conversely, dopamine participates in modulating synaptic

plasticity of medium spiny neurons which strongly express dopamine receptors in the striatum and nucleus accumbens.[67–69] In addition to dose-dependent effects of DYRK1A, DSCR1, and APP, the dysregulation of DAT1, DLK1, and VMAT2 expression may negatively modulate the dendritic development of DNs and other neuron subtypes in the DS brain through intracellular dopamine and ROS accumulation.

This study has a number of limitations. First, in DNs differentiated from SHEDs, it was difficult to analyze the axons and dendrites, as previously reported using MAP2 (dendrite marker) and Tau (axon marker).[29] Precise dendritic or synaptic complexity in a more mature stage has not been fully elucidated. Thus, functional defects in DS-DNs found in our system cannot be generalized to the neuropathology of DS. In addition, the expression of the postsynaptic scaffold protein PSD-95 was comparable between Ctrl-DNs and DS-DNs with potential defects in dendrites or synaptic complexity. To elucidate the defects of dopaminergic synapse formation, the localization of synaptic proteins, including PSD-95, should be further analyzed. Further studies with a large sample size are also warranted to visualize and quantitatively evaluate DN distributions in vivo using brain imaging techniques.[70] Second, molecular mechanisms underlying the altered expression of *DAT1*, *DLK1*, and *VMAT2* observed in DS-DNs remain elusive. Additional cofactors and/or epigenetic pathways involved in the unique expression mechanisms of each gene should be explored. Third, the contribution of VMAT2 in cytosolic dopamine and ROS regulation was not fully defined in this study. Mitochondrial dysfunction and excessive ROS generation, the underlying pathologies of DS, may also affect intracellular dopamine homeostasis, including accumulation of the highly reactive dopamine metabolites, such as 3,4-dihydroxyphenylacetaldehyde that can contribute to oxidative stress. Further efforts must be focused on identifying the exact role of VMAT2, enzymes, and metabolites on dopamine and ROS regulation. Fourth, the current study focused on male individuals with both X and Y chromosomes. Given the global epigenetic alterations caused by HSA21 trisomy, an analysis is also required using female individuals with two X chromosomes and no Y chromosome.

In conclusion, this study shows that in DS-DNs, the constitutive accumulation of intracellular dopamine and increased ROS levels are associated with *DAT1* upregulation as a result of *DLK1* downregulation. These events are relevant to mitochondrial dysfunction and oxidative stress, as well as impairments in neurite development, in DS-DNs. Our findings suggest that patient-derived SHEDs might be a useful cellular model to analyze the pathology of the dopaminergic system in the early developmental stage of DS.

CONFLICT OF INTEREST

The authors have stated explicitly that there are no conflicts of interest in connection with this article.

AUTHOR CONTRIBUTIONS

X. Sun and H. Kato planned and performed experiments, analyzed data, drafted and edited the manuscript, and approved the final version to be published. X. Han, H. Sato, and Y. Hirofuji analyzed data, reviewed and edited the manuscript, and approved the final version to be published. T. A. Kato, Y. Sakai, and S. Ohga reviewed and edited the manuscript and approved the final version to be published. S. Fukumoto and K. Masuda conceived and supervised the study, reviewed and edited the manuscript, and approved the final version to be published.

ORCID

Yasunari Sakai https://orcid.org/0000-0002-5747-8692

REFERENCES

1. Federico A, Cardaioli E, Da Pozzo P, Formichi P, Gallus GN, Radi E. Mitochondria, oxidative stress and neurodegeneration. *J Neurol Sci.* 2012;322:254-262.
2. Valenti D, de Bari L, De Filippis B, Henrion-Caude A, Vacca RA. Mitochondrial dysfunction as a central actor in intellectual disability-related diseases: an overview of Down syndrome, autism, Fragile X and Rett syndrome. *Neurosci Biobehav Rev.* 2014;46:202-217.
3. Izzo A, Mollo N, Nitti M, et al. Mitochondrial dysfunction in down syndrome: molecular mechanisms and therapeutic targets. *Mol Med.* 2018;24:2.
4. Valenti D, Braidy N, De Rasmo D, et al. Mitochondria as pharmacological targets in Down syndrome. *Free Radic Biol Med.* 2018;114:69-83.
5. Roizen NJ, Patterson D. Down's syndrome. *Lancet.* 2003;361:1281-1289.
6. Contestabile A, Benfenati F, Gasparini L. Communication breaks Down: from neurodevelopment defects to cognitive disabilities in Down syndrome. *Prog Neurobiol.* 2010;91:1-22.
7. Antonarakis SE, Lyle R, Dermitzakis ET, Reymond A, Deutsch S. Chromosome 21 and down syndrome: from genomics to pathophysiology. *Nat Rev Genet.* 2004;5:725-738.

8. Dekker AD, De Deyn PP, Rots MG. Epigenetics: the neglected key to minimize learning and memory deficits in Down syndrome. *Neurosci Biobehav Rev*. 2014;45:72-84.

9. Do C, Xing Z, Yu YE, Tycko B. Trans-acting epigenetic effects of chromosomal aneuploidies: lessons from Down syndrome and mouse models. *Epigenomics*. 2017;9:189-207.

10. Arenas E, Denham M, Villaescusa JC. How to make a midbrain dopaminergic neuron. *Development*. 2015;142:1918-1936.

11. Klein MO, Battagello DS, Cardoso AR, Hauser DN, Bittencourt JC, Correa RG. Dopamine: functions, signaling, and association with neurological diseases. *Cell Mol Neurobiol*. 2019;39:31-59.

12. Viggiano D, Vallone D, Sadile A. Dysfunctions in dopamine systems and ADHD: evidence from animals and modeling. *Neural Plast*. 2004;11:97-114.

13. Nguyen M, Roth A, Kyzar EJ, et al. Decoding the contribution of dopaminergic genes and pathways to autism spectrum disorder (ASD). *Neurochem Int*. 2014;66:15-26.

14. Oxelgren UW, Myrelid Å, Annerén G, et al. Prevalence of autism and attention-deficit-hyperactivity disorder in Down syndrome: a population-based study. *Dev Med Child Neurol*. 2017;59:276-283.

15. D'Amelio M, Puglisi-Allegra S, Mercuri N. The role of dopaminergic midbrain in Alzheimer's disease: Translating basic science into clinical practice. *Pharmacol Res*. 2018;130:414-419.

16. Yates CM, Simpson J, Gordon A, et al. Catecholamines and cholinergic enzymes in pre-senile and senile Alzheimer-type dementia and Down's syndrome. *Brain Res*. 1983;280:119-126.

17. Godridge H, Reynolds GP, Czudek C, Calcutt NA, Benton M. Alzheimer-like neurotransmitter deficits in adult Down's syndrome brain tissue. *J Neurol Neurosurg Psychiatry*. 1987;50:775-778.

18. Whittle N, Sartori SB, Dierssen M, Lubec G, Singewald N. Fetal Down syndrome brains exhibit aberrant levels of neurotransmitters critical for normal brain development. *Pediatrics*. 2007;120:e1465-e14671.

19. Dekker AD, Vermeiren Y, Albac C, et al. Aging rather than aneuploidy affects monoamine neurotransmitters in brain regions of Down syndrome mouse models. *Neurobiol Dis*. 2017;105:235-244.

20. Dekker AD, Vermeiren Y, Carmona-Iragui M, et al. Monoaminergic impairment in Down syndrome with Alzheimer's disease compared to early-onset Alzheimer's disease. *Alzheimers Dement (Amst)*. 2018;10:99-111.

21. Shimohata A, Ishihara K, Hattori S, et al. Ts1Cje Down syndrome model mice exhibit environmental stimuli-triggered locomotor hyperactivity and sociability concurrent with increased flux through central dopamine and serotonin metabolism. *Exp Neurol*. 2017;293:1-12.

22. Miura M, Gronthos S, Zhao M, et al. SHED: stem cells from human exfoliated deciduous teeth. *Proc Natl Acad Sci USA*. 2003;100:5807-5012.

23. Wang J, Wang X, Sun Z, et al. Stem cells from human-exfoliated deciduous teeth can differentiate into dopaminergic neuron-like cells. *Stem Cells Dev*. 2010;19:1375-1383.

24. Fujii H, Matsubara K, Sakai K, et al. Dopaminergic differentiation of stem cells from human deciduous teeth and their therapeutic benefits for Parkinsonian rats. *Brain Res*. 2015;1613:59-72.

25. Zhang N, Lu X, Wu S, et al. Intrastriatal transplantation of stem cells from human exfoliated deciduous teeth reduces motor defects in Parkinsonian rats. *Cytotherapy*. 2018;20:670-686.

26. Hirofuji S, Hirofuji Y, Kato H, et al. Mitochondrial dysfunction in dopaminergic neurons differentiated from exfoliated deciduous tooth-derived pulp stem cells of a child with Rett syndrome. *Biochem Biophys Res Commun*. 2018;498:898-904.

27. Nguyen HTN, Kato H, Masuda K, et al. Impaired neurite development associated with mitochondrial dysfunction in dopaminergic neurons differentiated from exfoliated deciduous tooth-derived pulp stem cells of children with autism spectrum disorder. *Biochem Biophys Rep*. 2018;16:24-31.

28. Nguyen HTN, Kato H, Sato H, et al. Positive effect of exogenous brain-derived neurotrophic factor on impaired neurite development and mitochondrial function in dopaminergic neurons derived from dental pulp stem cells from children with attention deficit hyperactivity disorder. *Biochem Biophys Res Commun*. 2019;513:1048-1054.

29. Pham TTM, Kato H, Yamaza H, et al. Altered development of dopaminergic neurons differentiated from stem cells from human exfoliated deciduous teeth of a patient with Down syndrome. *BMC Neurol*. 2018;18:132.

30. Masuda K, Han X, Kato H, et al. Dental pulp-derived mesenchymal stem cells for modeling genetic disorders. *Int J Mol Sci*. 2021;22:2269.

31. Li X, Yu Y, Gorshkov B, et al. Hsp70 suppresses mitochondrial reactive oxygen species and preserves pulmonary microvascular barrier integrity following exposure to bacterial toxins. *Front Immunol*. 2018;9:1039.

32. Jang S, Javadov S. Elucidating the contribution of ETC complexes I and II to the respirasome formation in cardiac mitochondria. *Sci Rep*. 2018;8:17732.

33. Sun X, Kato H, Sato H, et al. Impaired neurite development and mitochondrial dysfunction associated with calcium accumulation in dopaminergic neurons differentiated from the dental pulp stem cells of a patient with metatropic dysplasia. *Biochem Biophys Rep*. 2012;26:100968.

34. Kawashima N. Characterisation of dental pulp stem cells: a new horizon for tissue regeneration? *Arch Oral Biol*. 2012;57:1439-1458.

35. Mann DM, Lincoln J, Yates PO, Brennan CM. Monoamine metabolism in Down syndrome. *Lancet*. 1980;316:1366-1367.

36. Kay AD, Schapiro MB, Riker AK, Haxby JV, Rapoport SI, Cutler NR. Cerebrospinal fluid monoaminergic metabolites are elevated in adults with Down's syndrome. *Ann Neurol*. 1987;21:408-411.

37. Smits SM, Ponnio T, Conneely OM, Burbach JP, Smidt MP. Involvement of Nurr1 in specifying the neurotransmitter identity of ventral midbrain dopaminergic neurons. *Eur J Neurosci*. 2003;18:1731-1738.

38. Jacobs FM, van Erp S, van der Linden AJ, von Oerthel L, Burbach JP, Smidt MP. Pitx3 potentiates Nurr1 in dopamine neuron terminal differentiation through release of SMRT-mediated repression. *Development*. 2009;136:531-540.

39. Jacobs FM, van der Linden AJ, et al. Identification of Dlk1, Ptpru and Klhl1 as novel Nurr1 target genes in meso-diencephalic dopamine neurons. *Development*. 2009;136:2363-2373.

40. Smas CM, Sul HS. Pref-1, a protein containing EGF-like repeats, inhibits adipocyte differentiation. *Cell*. 1993;73:725-734.

41. Laborda J, Sausville EA, Hoffman T, Notario V. dlk, a putative mammalian homeotic gene differentially expressed in small

cell lung carcinoma and neuroendocrine tumor cell line. *J Biol Chem*. 1993;268:3817-3820.

42. Laborda J. The role of the epidermal growth factor-like protein dlk in cell differentiation. *Histol Histopathol*. 2000;15:119-129.

43. Falix FA, Aronson DC, Lamers WH, Gaemers IC. Possible roles of DLK1 in the Notch pathway during development and disease. *Biochim Biophys Acta*. 2012;1822:988-995.

44. Traustadóttir GÁ, Lagoni LV, Ankerstjerne LBS, Bisgaard HC, Jensen CH, Andersen DC. The imprinted gene Delta like noncanonical Notch ligand 1 (Dlk1) is conserved in mammals, and serves a growth modulatory role during tissue development and regeneration through Notch dependent and independent mechanisms. *Cytokine Growth Factor Rev*. 2019;46:17-27.

45. Bauer M, Szulc J, Meyer M, et al. Delta-like 1 participates in the specification of ventral midbrain progenitor derived dopaminergic neurons. *J Neurochem*. 2008;104:1101-1115.

46. Fischer DF, van Dijk R, Sluijs JA, et al. Activation of the Notch pathway in Down syndrome: cross-talk of Notch and APP. *FASEB J*. 2005;19:1451-1458.

47. Lockstone HE, Harris LW, Swatton JE, Wayland MT, Holland AJ, Bahn S. Gene expression profiling in the adult Down syndrome brain. *Genomics*. 2007;90:647-660.

48. Fernandez-Martinez J, Vela EM, Tora-Ponsioen M, Ocaña OH, Nieto MA, Galceran J. Attenuation of Notch signalling by the Down-syndrome-associated kinase DYRK1A. *J Cell Sci*. 2009;122:1574-1583.

49. Czermiński JT, Lawrence JB. Silencing trisomy 21 with XIST in neural stem cells promotes neuronal differentiation. *Dev Cell*. 2020;52:294-308.e3.

50. da Rocha ST, Edwards CA, Ito M, Ogata T, Ferguson-Smith AC. Genomic imprinting at the mammalian Dlk1-Dio3 domain. *Trends Genet*. 2008;24:306-316.

51. Kagami M, Mizuno S, Matsubara K, et al. Epimutations of the IG-DMR and the MEG3-DMR at the 14q32.2 imprinted region in two patients with Silver-Russell Syndrome-compatible phenotype. *Eur J Hum Genet*. 2015;23:1062-1067.

52. Lu J, Mccarter M, Lian G, et al. Global hypermethylation in fetal cortex of Down syndrome due to DNMT3L overexpression. *Hum Mol Genet*. 2016;25:1714-1727.

53. Laufer BI, Hwang H, Vogel Ciernia A, Mordaunt CE, LaSalle JM. Whole genome bisulfite sequencing of Down syndrome brain reveals regional DNA hypermethylation and novel disorder insights. *Epigenetics*. 2019;14:672-684.

54. Sørensen KD, Wild PJ, Mortezavi A, et al. Genetic and epigenetic SLC18A2 silencing in prostate cancer is an independent adverse predictor of biochemical recurrence after radical prostatectomy. *Clin Cancer Res*. 2009;15:1400-1410.

55. Haldrup C, Lynnerup AS, Storebjerg TM, et al. Large-scale evaluation of SLC18A2 in prostate cancer reveals diagnostic and prognostic biomarker potential at three molecular levels. *Mol Oncol*. 2016;10:825-837.

56. Sotnikova TD, Beaulieu JM, Gainetdinov RR, Caron MG. Molecular biology, pharmacology and functional role of the plasma membrane dopamine transporter. *CNS Neurol Disord Drug Targets*. 2006;5:45-56.

57. Erickson JD, Eiden LE. Functional identification and molecular cloning of a human brain vesicle monoamine transporter. *J Neurochem*. 1993;61:2314-2317.

58. Guillot TS, Miller GW. Protective actions of the vesicular monoamine transporter 2 (VMAT2) in monoaminergic neurons. *Mol Neurobiol*. 2009;39:149-170.

59. Masoud ST, Vecchio LM, Bergeron Y, et al. Increased expression of the dopamine transporter leads to loss of dopamine neurons, oxidative stress and l-DOPA reversible motor deficits. *Neurobiol Dis*. 2015;74:66-75.

60. Lohr KM, Masoud ST, Salahpour A, Miller GW. Membrane transporters as mediators of synaptic dopamine dynamics: implications for disease. *Eur J Neurosci*. 2017;45:20-33.

61. Chen Y, Wang Y, Chen J, et al. Roles of transcriptional corepressor RIP140 and coactivator PGC-1alpha in energy state of chronically infarcted rat hearts and mitochondrial function of cardiomyocytes. *Mol Cell Endocrinol*. 2012;362:11-18.

62. Piccoli C, Izzo A, Scrima R, et al. Chronic pro-oxidative state and mitochondrial dysfunctions are more pronounced in fibroblasts from Down syndrome foeti with congenital heart defects. *Hum Mol Genet*. 2013;22:1218-1232.

63. Izzo A, Manco R, Bonfiglio F, et al. NRIP1/RIP140 siRNA-mediated attenuation counteracts mitochondrial dysfunction in Down syndrome. *Hum Mol Genet*. 2014;23:4406-4419.

64. Benavides-Piccione R, Ballesteros-Yáñez I, de Lagrán MM, et al. On dendrites in Down syndrome and DS murine models: a spiny way to learn. *Prog Neurobiol*. 2004;74:111-126.

65. Cheng A, Hou Y, Mattson MP. Mitochondria and neuroplasticity. *ASN Neuro*. 2010;2:e00045.

66. Lefebvre JL, Sanes JR, Kay JN. Development of dendritic form and function. *Annu Rev Cell Dev Biol*. 2015;31:741-777.

67. Surmeier DJ, Ding J, Day M, Wang Z, Shen W. D1 and D2 dopamine-receptor modulation of striatal glutamatergic signaling in striatal medium spiny neurons. *Trends Neurosci*. 2007;30:228-235.

68. Yao WD, Spealman RD, Zhang J. Dopaminergic signaling in dendritic spines. *Biochem Pharmacol*. 2008;75:2055-2069.

69. Yagishita S, Hayashi-Takagi A, Ellis-Davies GCR, Urakubo H, Ishii S, Kasai H. A critical time window for dopamine actions on the structural plasticity of dendritic spines. *Science*. 2014;345:1616-1620.

70. Chalon S, Vercouillie J, Payoux P, et al. The story of the dopamine transporter PET tracer LBT-999: from conception to clinical use. *Front Med (Lausanne)*. 2019;6:90.

SUPPORTING INFORMATION

Additional supporting information may be found in the online version of the article at the publisher's website.